Impact of relative permeability hysteresis on geological CO_2 storage

R. Juanes,[1] E. J. Spiteri,[2] F. M. Orr Jr.,[3] and M. J. Blunt[4]

Received 13 December 2005; revised 28 July 2006; accepted 21 August 2006; published 23 December 2006.

[1] Relative permeabilities are the key descriptors in classical formulations of multiphase flow in porous media. Experimental evidence and an analysis of pore-scale physics demonstrate conclusively that relative permeabilities are not single functions of fluid saturations and that they display strong hysteresis effects. In this paper, we evaluate the relevance of relative permeability hysteresis when modeling geological CO_2 sequestration processes. Here we concentrate on CO_2 injection in saline aquifers. In this setting the CO_2 is the nonwetting phase, and capillary trapping of the CO_2 is an essential mechanism after the injection phase during the lateral and upward migration of the CO_2 plume. We demonstrate the importance of accounting for CO_2 trapping in the relative permeability model for predicting the distribution and mobility of CO_2 in the formation. We conclude that modeling of relative permeability hysteresis is required to assess accurately the amount of CO_2 that is immobilized by capillary trapping and therefore is not available to leak. We also demonstrate how the mechanism of capillary trapping can be exploited (e.g., by controlling the injection rate or alternating water and CO_2 injection) to improve the overall effectiveness of the injection project.

Citation: Juanes, R., E. J. Spiteri, F. M. Orr Jr., and M. J. Blunt (2006), Impact of relative permeability hysteresis on geological CO_2 storage, *Water Resour. Res.*, *42*, W12418, doi:10.1029/2005WR004806.

1. Introduction

[2] There is little doubt that human socioeconomic activities are interacting with the biogeochemistry of the planet at a global scale. One example is the impact of carbon dioxide atmospheric emissions on the global carbon cycle [*Falkowski et al.*, 2000]. The result of anthropogenic releases is an accumulation of carbon dioxide in the atmosphere, accompanied by a reduction in the pH of the upper ocean [*Intergovernmental Panel on Climate Change*, 1996]. It is also well documented that carbon dioxide is a greenhouse gas, and one of the main contributors to global warming [*Falkowski et al.*, 2000; *Cox et al.*, 2000]. Current predictions suggest that, unless an aggressive reduction of net CO_2 emissions is implemented, carbon dioxide concentrations in the atmosphere will continue to rise during this century [*Wigley et al.*, 1996; *Hoffert et al.*, 1998]. Since anthropogenic CO_2 emissions are primarily due to energy consumption, and 85% of the primary power is supplied by fossil fuels now, a drastic reduction in CO_2 emissions represents a major challenge [*Orr*, 2004].

[3] CO_2 sequestration refers to the capture and long-term storage of anthropogenic CO_2 in order to limit its emission to the atmosphere [*Lackner*, 2003]. Injection into geological formations is one option to store CO_2 [*Hitchon et al.*, 1999; *Bachu*, 2000; *Orr*, 2004]. Different target formations have been identified for this purpose, including depleted oil and gas reservoirs [*Holloway*, 2001; *Kovscek and Wang*, 2005; *Kovscek and Cakici*, 2005], unminable coal beds [*Bromhal et al.*, 2005], and deep saline aquifers [*Bruant et al.*, 2002; *Pruess and García*, 2002; *Pruess et al.*, 2003; *Bachu*, 2003].

[4] One of the major concerns in any sequestration project is the potential leakage of the CO_2 into the atmosphere. Possible causes of leaks are loss of integrity of the cap rock due to overpressurization of the geological formation [*Rutqvist and Tsang*, 2002; *Jimenez and Chalaturnyk*, 2002], and abandoned wells that may be present [*Nordbotten et al.*, 2004]. When planning geologic sequestration projects in saline aquifers or depleted hydrocarbon reservoirs, it is therefore essential to predict the migration and distribution of the CO_2 in the subsurface structure so that injection can be maximized while keeping the risk of leakage at a minimum.

[5] In this investigation we consider injection and storage of CO_2 in saline aquifers. Many authors have presented simulations of CO_2 injection and migration [see, e.g., *Johnson et al.*, 2000; *Ennis-King and Paterson*, 2002; *Wellman et al.*, 2003; *Pruess et al.*, 2003; *Xu et al.*, 2003; *Doughty and Pruess*, 2004; *Flett et al.*, 2004; *Kumar et al.*, 2005; *Mo and Akervoll*, 2005; *Obi and Blunt*, 2006] using a variety of approaches. Because of the density difference between the CO_2 and the brine, the low viscosity CO_2 tends to migrate to the top of the geologic structure. This upward migration is sometimes delayed or suppressed by low permeability layers that impede the vertical flow of gas (in this paper we often refer to the CO_2 phase as gas even

[1]Department of Civil and Environmental Engineering, Massachusetts Institute of Technology, Cambridge, Massachusetts, USA.
[2]Chevron Energy Technology Company, Houston, Texas, USA.
[3]Department of Petroleum Engineering, Stanford University, Stanford, California, USA.
[4]Department of Earth Science and Engineering, Imperial College London, London, UK.

0043-1397/06/2005WR004806$09.00

though, in practice, it is typically present as a supercritical fluid). There are several mechanisms by which the CO_2 can be stored, which include the following. (1) In hydrodynamic trapping, the buoyant CO_2 remains as a mobile fluid but is prevented from flowing back to the surface by an impermeable cap rock [*Bachu et al.*, 1994]. (2) In solution trapping, dissolution of the CO_2 in the brine [*Pruess and García*, 2002], possibly enhanced by gravity instabilities due to the larger density of the brine–CO_2 liquid mixture [*Ennis-King and Paterson*, 2005; *Ennis-King et al.*, 2005; *Riaz et al.*, 2006]. (3) In mineral trapping, geochemical binding to the rock due to mineral precipitation [*Gunter et al.*, 1997; *Pruess et al.*, 2003]. Finally, (4) in capillary trapping, disconnection of the CO_2 phase into an immobile (trapped) fraction [*Kumar et al.*, 2005; *Flett et al.*, 2004; *Spiteri et al.*, 2005].

[6] In this paper we demonstrate that the picture that emerges from the first three sequestration mechanisms, permeability, dissolution and mineral trapping, is incomplete. What is missing is consideration of the irreversibility of multiphase flow dynamics and, in particular, relative permeability hysteresis and physical trapping of the CO_2 phase within the porous medium. During the injection period, the less wetting CO_2 displaces the more wetting brine in a drainage-like process. However, after injection, the buoyant CO_2 migrates laterally and upward, and water displaces CO_2 at the trailing edge of the plume in an imbibition-like process. This leads to disconnection of the once-continuous plume into blobs and ganglia, which are effectively immobile [*Hunt et al.*, 1988]. It is this sequestration mechanism, capillary or residual trapping of CO_2 in its own immobile phase, that we emphasize in this investigation. We show that the capillary trapping mechanism has a huge impact on the migration and distribution of CO_2 which, in turn, affects the effectiveness of the other sequestration mechanisms.

[7] The importance of the "residual" CO_2 saturation has been pointed out by *Doughty and Pruess* [2004] and *Hovorka et al.* [2004], with reference to laboratory and field data from the Frio brine pilot experiment. However, no distinction was made between critical saturation (during drainage) and residual saturation (during imbibition) in their simulations. *Kumar et al.* [2005] performed a study of CO_2 storage in saline aquifers that accounted for dissolution and chemical reaction. They considered relative permeability hysteresis using a Land-type model. They concluded that the effect of residual gas on CO_2 storage can be very large and more significant than sequestration as brine or mineral. Their results indicated that significant capillary trapping of CO_2 occurred during the injection phase. However, injection is a drainage process, and gas is not trapped during drainage: Residual gas is formed after injection stops when water displaces CO_2. Postinjection trapping was analyzed in the recent study by *Flett et al.* [2004], who used a Land hysteresis model and emphasized the sensitivity of the predictions to the choice of the Land trapping parameter. In our simulations we will confirm that trapping is a significant storage process, but only after the initial injection phase.

[8] There seems to be some consensus that the timescales associated with each of the sequestration mechanisms are very different [*Pruess et al.*, 2003]. Residual and hydrodynamic trapping occur on small timescales, dictated by the two-phase flow dynamics. Despite the fact that dissolution into the aqueous phase can be considered as an equilibrium process locally, it can be slow at the aquifer scale because it relies on the diffusion of CO_2 to regions not in contact with the CO_2 plume. Unstable gravity-driven convection can increase the rate of dissolution (because brine saturated with CO_2 is slightly more dense than brine alone), but the estimates of *Ennis-King and Paterson* [2005] and *Riaz et al.* [2006] indicate that the increase is significant only in relatively high permeability formations. Mineral trapping is believed to be a very slow process, because of the slow kinetics of precipitation reactions [*Knauss et al.*, 2005]. Therefore it is not unlikely that the timescale for mineral trapping is at least an order of magnitude larger than that of solution trapping, which may easily be an order of magnitude larger than that of hydrodynamic and residual trapping. As a result, we investigate the effects of capillary and hydrodynamic trapping alone, and we establish that relative permeability hysteresis becomes a major factor in the assessment of CO_2 sequestration projects. Moreover, we elucidate how the irreversible character of two-phase flow can be exploited to maximize residual trapping and subsequently increase CO_2 storage.

[9] An outline of the paper is as follows. In section 2 we give an account of the phenomenon of hysteresis from a pore-scale viewpoint, and explain what is the physical basis for residual trapping in aquifer disposal of CO_2. In section 3 we describe the setup of the numerical simulations employed to assess the importance of hysteresis. We used a realistic three-dimensional heterogeneous formation, as well as measured relative permeability data that display hysteresis. The results of the simulations are discussed in section 4. Finally, in section 5, we gather the main conclusions of this investigation.

2. Trapping and Relative Permeability Hysteresis

[10] Hysteresis refers to irreversibility, or path dependence. In multiphase flow, it manifests itself through the dependence of the relative permeabilities and capillary pressures on the saturation path and the saturation history. From the point of view of pore-scale processes, hysteresis has at least two sources [*de Gennes et al.*, 2004]. (1) The first source is contact angle hysteresis: the advancing contact angle (of wetting phase displacing a nonwetting phase) is larger than the receding contact angle (of wetting phase retreating by nonwetting phase invasion) due to chemical heterogeneities or surface roughness. (2) The second source is trapping of the nonwetting phase: during an imbibition process, a fraction of the nonwetting phase gets disconnected in the form of blobs or ganglia, becoming effectively immobile (trapped). Hysteresis effects are larger in processes with strong flow reversals. This is the case of cyclic water and gas injection in a porous medium, in which the gas phase is trapped during water injection after a gas flood.

2.1. Pore-Scale View of the Hysteresis Phenomenon

[11] Trapping and hysteresis have been successfully explained in terms of the displacement mechanisms that take place at the pore scale [*Lenormand et al.*, 1983], and successfully modeled using pore-network simulation tools

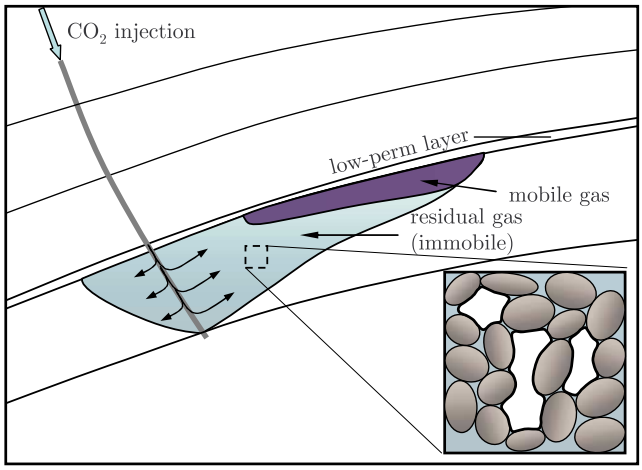

Figure 1. Schematic of the trail of residual CO_2 that is left behind because of snap-off as the plume migrates upward during the postinjection period.

[e.g., *Jerauld and Salter*, 1990; *Valvatne and Blunt*, 2004]. Consider a medium that is initially filled with water. The solid grains are made of minerals that are naturally wetting to water and, therefore the medium is water wet. During CO_2 injection into the aquifer, the nonwetting CO_2 phase invades the pore space. This is a drainage process in which the only mechanism for displacement of water by CO_2 is piston-type displacement: the CO_2 invades the porous medium in the form of a continuous, connected cluster. Water, however, remains present not only in small pores that have not been filled with CO_2 but also in the corners and crevices of the pores that have been invaded. Consider now the displacement of the CO_2 by water. During this process, there are several physical mechanisms by which the water can displace the CO_2 [*Lenormand et al.*, 1983]. In addition to piston-type displacement, cooperative pore-body filling and snap-off may occur. For water wet rocks, snap-off is the dominant mechanism [*Al-Futaisi and Patzek*, 2003; *Valvatne and Blunt*, 2004]. The important point is that snap-off and cooperative filling may lead to disconnection and bypassing of the CO_2. The macroscopic consequences of these pore-scale processes are trapping and relative permeability hysteresis. In accordance with the pore-scale explanation give above, experimental data strongly suggest that the nonwetting phase experiences much more pronounced hysteresis than the wetting phase. Several hysteresis empirical models have been developed to characterize the relative permeabilities and trapped saturation of the nonwetting phase after a flow reversal [*Land*, 1968; *Killough*, 1976; *Carlson*, 1981; *Lenhard and Parker*, 1987; *Jerauld*, 1997; *Larsen and Skauge*, 1998; *Lenhard and Oostrom*, 1998; *Blunt*, 2000].

2.2. Basis for Residual Trapping in Geologic CO_2 Storage

[12] Saline aquifers, predominantly water wet, are prime candidates for geologic CO_2 sequestration. In water wet media and a capillary-dominated flow regime, snap-off is the dominant trapping mechanism at the pore scale. Capillary trapping of the nonwetting gas phase occurs during water flooding when the gas saturation is decreasing, and the water saturation increases as it invades the pore space. During the injection of CO_2 in the geologic formation, the gas saturation increases in a drainage-like process. Vertical flow paths are created as the gas phase migrates laterally away from the injection wells and to the top of the aquifer due to buoyancy forces. Once the injection stops, the CO_2 continues to migrate upward. At the leading edge of the CO_2 plume, gas continues to displace water in a drainage process (increasing gas saturation), while at the trailing edge water displaces gas in an imbibition process (increasing water saturations). The presence of an imbibition saturation path leads to snap-off and, subsequently, trapping of the gas phase. A trail of residual, immobile CO_2 is left behind the plume as it migrates upward (Figure 1).

3. Numerical Simulations

[13] We perform a series of representative simulations to assess the impact of residual trapping and relative permeability hysteresis on the migration and distribution of injected CO_2 in a sequestration project. We used the commercial reservoir simulator Eclipse 100 [*Schlumberger*, 2005].

3.1. Reservoir Description

[14] We carried out simulations of CO_2 injection in a synthetic but realistic model of a geologic formation. Since the formation is relatively small, these simulations are representative of a CO_2 pilot test, rather than a full-field CO_2 sequestration project. The objective is to illustrate the importance of the physical processes considered, although in section 5 we discuss their implications at a more realistic operational scale. We selected the PUNQ-S3 model, which is a geometrically complex and heterogeneous three-dimensional geologic model originally designed as a test case for oil production forecasting under uncertainty. The original PUNQ-S3 model is described in detail elsewhere [*Floris et al.*, 2001], and the model data are publicly available for download (Netherlands Institute of Applied Geosciences, PUNQ case Studies, http://www.nitg.tno.nl/punq/cases/index.shtml). We modified the original model slightly to study hysteresis and trapping effects in a CO_2 injection scenario. The modifications were limited to the well locations and flow rates, the fluid properties, the depth of the formation, and the relative permeability tables. The geometry of the model is characterized by a dome in the center and contains five layers of fluvial sand and shale. We set the top of the formation at a depth of 840 m. The average reservoir thickness is about 15 m. The formation is discretized into $19 \times 28 \times 5$ grid blocks, of which 1761 blocks are active. The x and y dimension of each block is 180 m. The average porosity is 0.2, and the average horizontal permeability is 100 md = 10^{-13} m^2. The permeability anisotropy ratio is about 3. A map of the horizontal permeability is shown in Figure 2.

[15] The aquifer pore volume is approximately 3.6×10^6 m^3 with an initial pressure of 90 bar at the top of the structure and a temperature of 40°C. These pressure and temperature conditions ensure that the CO_2 is present as a supercritical fluid. Our model has eight injection wells open to the bottom layer of the aquifer. The injection wells are rate controlled and operate with a constraint in the maximum bottom hole pressure of 160 bar, which is never reached. The well terms are handled in a fully implicit

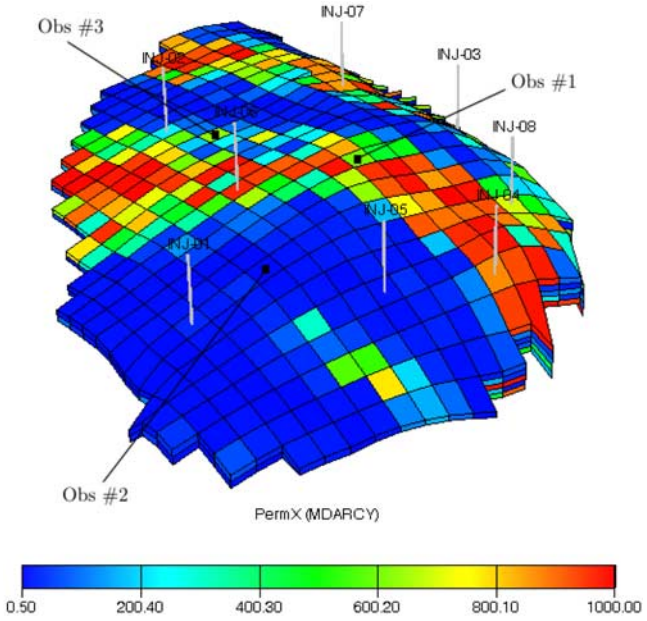

Figure 2. Horizontal permeability distribution (1 md = 10^{-15} m^2) of the PUNQ-S3 model. Also shown are the injection wells and the "observation" grid blocks.

fashion, using the default well model in Eclipse. In order to model boundary conditions that are representative of an aquifer that extends beyond the simulation grid, we assign a very large pore volume to the boundary blocks. Specifically, we multiply the pore volume of these blocks by a factor of 1000. While this approach certainly cannot capture the flow dynamics associated with the surrounding aquifer, it has proved to be effective in practice. Upon CO_2 injection, it allows that the brine leave the system, while reproducing a modest pressure buildup at the boundary.

3.2. Trapping and Relative Permeability Hysteresis Models

[16] The relative permeabilities of water and gas are taken from *Oak* [1990] for a water wet Berea sandstone and a gas-water system. Evaluation of the relative permeabilities in Eclipse was performed by linear interpolation between data points. The relative permeability curves are shown in Figure 3. Because the medium is strongly water wet, hysteresis effects are significant in the gas relative permeability only. The relative permeability data of *Oak* [1990] were measured for a brine–nitrogen gas system under low pore pressure and, admittedly, may not be entirely appropriate for a system with supercritical CO_2. The value of residual gas saturation of 40%, however, is in the range of experimental values of *Bennion and Bachu* [2006].

[17] The most important quantity determining the significance of hysteresis effects is the trapped gas saturation after a flow reversal (from drainage to imbibition). A trapping model attempts to relate the trapped (residual) gas saturation to the maximum gas saturation, that is, the actual gas saturation at flow reversal. Most relative permeability hysteresis models make use of the trapping model proposed by *Land* [1968]. In this model, the trapped gas saturation S_{gt} is computed as

$$S_{gt} = \frac{S_{gi}}{1 + CS_{gi}}, \tag{1}$$

where S_{gi} is the initial gas saturation (actual gas saturation at flow reversal) and C is the Land trapping coefficient. The Land trapping coefficient is computed from the bounding drainage and imbibition relative permeability curves as follows:

$$C = \frac{1}{S_{gt,\max}} - \frac{1}{S_{g,\max}}, \tag{2}$$

where $S_{g,\max}$ is the maximum gas saturation, and $S_{gt,\max}$ is the maximum trapped saturation, associated with the bounding imbibition curve. All these quantities are illustrated in Figure 4. The Land trapping model has been validated by comparison with experiments [*Land*, 1968; *Jerauld*, 1997; *Spiteri and Juanes*, 2006] and pore-network simulations [*Spiteri et al.*, 2005] for water wet rocks. The bounding drainage and imbibition curves from the experimental data (Figure 3) result in a Land trapping coefficient $C \approx 1$.

[18] A relative permeability hysteresis model characterizes the scanning curves during imbibition and drainage cycles. In this paper, we have used the *Killough* [1976]

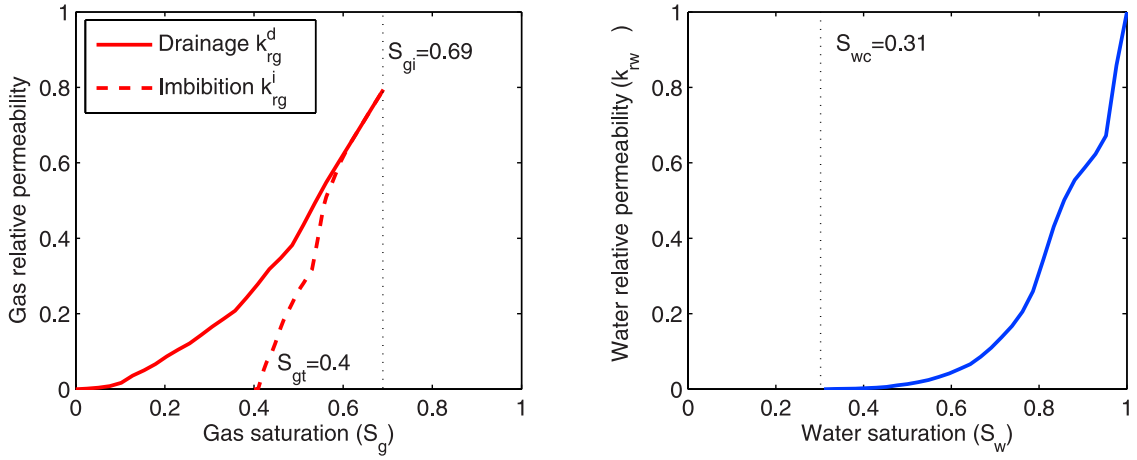

Figure 3. Relative permeability curves used in the CO_2 simulations, taken from *Oak* [1990] for a water wet Berea sandstone.

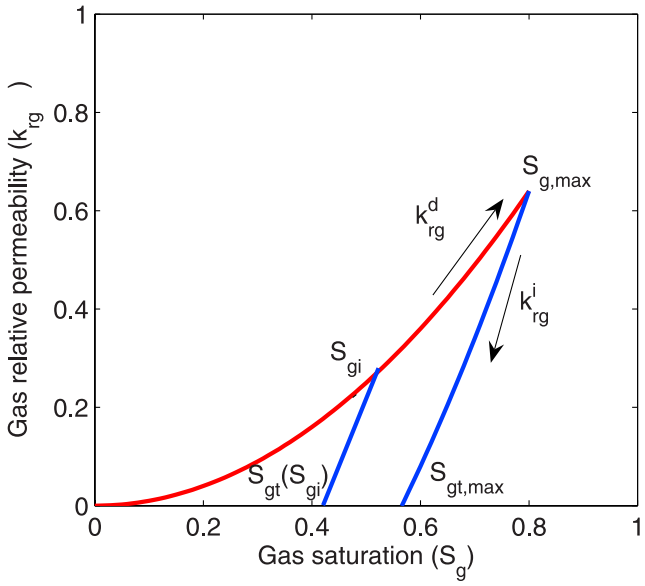

Figure 4. Parameters required in the evaluation and application of the Land trapping model.

hysteresis model. In Killough's method, the gas relative permeability along a scanning curve, such as the one depicted in Figure 4, is computed as:

$$k^i_{rg}(S_g) = k^{ib}_{rg}\left(S^*_g\right)\frac{k^d_{rg}(S_{gi})}{k^d_{rg}(S_{gi,\max})}, \tag{3}$$

where

$$S^*_g = S_{gt,\max} + \frac{(S_g - S_{gt})(S_{gi,\max} - S_{gt,\max})}{S_{gi} - S_{gt}}. \tag{4}$$

In equation (3), k^d_{rg} and k^{ib}_{rg} represent the bounding drainage and imbibition curves, respectively. The bounding imbibition curve is assumed to be available from experiments, or computed using Land's imbibition model [*Land*, 1968]. In Killough's model, scanning curves are assumed to be "reversible", so that the imbibition curve is representative of a subsequent drainage process.

[19] Of course, capillary pressure–saturation relationships also exhibit marked hysteresis effects. Several mathematical models exist to treat hysteretic capillary pressure curves, including the one proposed by *Killough* [1976]. From a practical point of view, however, capillary pressure effects are often negligible at the time of numerically simulating field-scale displacements, especially, as is the case here, when the characteristic capillary length is much smaller than the grid resolution [*Aziz and Settari*, 1979; *Spiteri and Juanes*, 2006]. We have indeed checked that our predictions are insensitive to the choice of the hysteretic or nonhysteretic capillary pressure curves. As a result, capillary pressure was assumed to be zero in the simulations presented here.

3.3. Fluid Properties

[20] We have used fluid properties that are representative of water and CO_2 at reservoir conditions [*McCain*, 1990; *Garcia*, 2003]. The phase behavior of the system is greatly simplified by the assumption that the two fluids are immiscible.

[21] Assuming a concentration of total dissolved solids of about 5%, we used a value of 1030 kg m^{-3} for the density of water at standard conditions. A constant value of water compressibility 4.35 $\times$ 10^{-5} bar^{-1} was employed. For a reference pressure of 130 bar and a reference temperature of 40°C, the dynamic viscosity of water is approximately 0.81 $\times$ 10^{-3} kg m^{-1} s^{-1}. We assumed a linear dependence of water viscosity with pressure, with a viscosibility

$$\frac{1}{\mu_w}\frac{\partial \mu_w}{\partial p} = 7.4 \times 10^{-4} \ \text{bar}^{-1}. \tag{5}$$

[22] We relied on the compilation and analysis of *Garcia* [2003] for the determination of appropriate CO_2 properties at reservoir conditions. From the density at reservoir and surface conditions, one can determine the CO_2 formation volume factor B_g, which is defined as the volume of CO_2 at reservoir conditions corresponding to a unit volume of CO_2 at surface (standard) conditions. Thus

$$B_g = \frac{V_{\text{res}}}{V_{\text{sc}}} = \frac{\rho_{\text{sc}}}{\rho_{\text{res}}}. \tag{6}$$

In Table 1 we list the density, formation volume factor and dynamic viscosity of CO_2 at 40°C as a function of pressure. Linear interpolation between values in Table 1 was used in the simulations.

3.4. Setup of Numerical Simulations

[23] The formation is initially filled with brine. CO_2 injection is simulated by controlling the volume of CO_2 that is injected into the formation. A total of 0.15 pore volumes are injected into the bottom layer of the aquifer. The injection rate and volume are the same for all eight injectors.

[24] We simulated four different scenarios, summarized in Table 2. They were designed to assess the following factors: (1) hysteresis and trapping, by comparing the results of case 2 (in which hysteresis is modeled) and case 1 (in which hysteresis is not modeled); (2) injection rate, by comparing the results of case 2 (CO_2 injection during 10 years) and case 3 (injection of the same volume over a period of 50 years); and (3) injection of water, by comparing case 4 (injection of 0.05 pore volumes of water after 5 and 10 years of CO_2 injection) with case 2, respectively (injection of CO_2 alone).

[25] For each case, we show results of the fluid distribution after 500 years from the beginning of the injection phase. We

Table 1. CO_2 Properties at 40°C

Pressure, bars	Density, kg m^{-3}	Formation Volume Factor	Viscosity, $\times 10^{-3}$ kg m^{-1} s^{-1}
1	1.8	1.00000	
80	234	0.00769	0.0325
100	447	0.00403	0.0525
120	632	0.00285	0.0625
160	747	0.00241	0.0725
200	803	0.00224	0.0800
300	883	0.00204	0.0950

Table 2. Summary of CO_2 Sequestration Simulations

Case	Description	Injection Scheme	Injection Time
1	no hysteresis	0.15 PV CO_2	10 yr
2	hysteresis	0.15 PV CO_2	10 yr
3	hysteresis	0.15 PV CO_2	50 yr
4	hysteresis – WAG	0.075 PV CO_2, 0.05 PV water	5 yr, 1 yr
		0.075 PV CO_2, 0.05 PV water	5 yr, 1 yr

plot three-dimensional views of the CO_2 saturation. Additional insight into the dynamic behavior of the system is gained by plotting the evolution of the actual CO_2 saturation and the trapped CO_2 saturation at specific grid blocks. We chose three "observation" points: one near the top of the anticline structure (observation point 1, grid block 13,18,1), one at a slightly lower elevation (observation point 2, grid block 7,21,1), and a third one at a lower elevation still (observation point 3, grid block 11,11,1). All of them are located at the top layer of the formation. The location of the injection wells and the observation grid blocks is shown in Figure 2.

4. Results and Discussions

4.1. Effect of Hysteresis and Trapping

[26] We begin by illustrating the dramatic effect of relative permeability hysteresis on the predictions of the fate of the injected CO_2. We compare the results from case 1 (no hysteresis) and case 2 (with hysteresis). In case 1, the gas relative permeability is assumed to be reversible, and only the drainage curve is used. Both cases simulate injection of a total of 0.15 pore volumes of CO_2 during 10 years, and the migration of the CO_2 plume during the next 490 years.

[27] In Figure 5 we plot the distribution of CO_2 saturation predicted by both models after 500 years from the beginning of injection. In case 1, because the gas relative permeability is assumed to be reversible, the model does not predict any trapping of CO_2. The CO_2 plume migrates upward due to buoyancy forces without leaving any residual saturation behind. After a sufficiently long time, the model predicts the formation of a gas cap of mobile CO_2 at the top of the formation. This scenario is unfavorable from a sequestration standpoint: damage in the cap rock could lead to fractures that might serve as conduits for leaks of the mobile CO_2 to upper formations and, eventually, the atmosphere.

[28] The predictions under case 2 are entirely different. After the injection phase, the model predicts a trail of residual, immobile CO_2 during the migration of the plume. As a result, while there is a net flow of CO_2 in the vertical direction, trapping prevents the injected CO_2 from forming a gas cap. In fact, the simulation predicts that, after 500 years or less, almost all the CO_2 is trapped in the formation. Accounting for hysteresis effects leads to a spread out distribution of trapped CO_2, as opposed to a concentrated distribution of mobile CO_2. This scenario is in fact much more realistic and, importantly, much more favorable for the effectiveness of CO_2 sequestration: it minimizes the risk of leaks (the gas is immobile) and enhances other sequestration mechanisms such as dissolution into the brine and geochemical binding (more interfacial area between the CO_2 and the initial pore water).

[29] Figure 6 shows the evolution of the actual CO_2 saturation with time at the three different observation grid blocks in the aquifer during the first 200 years. For the block at the very top (observation point 1) we see the accumulation of CO_2 when hysteresis effects are ignored, reaching a saturation value close to 0.7 that corresponds to

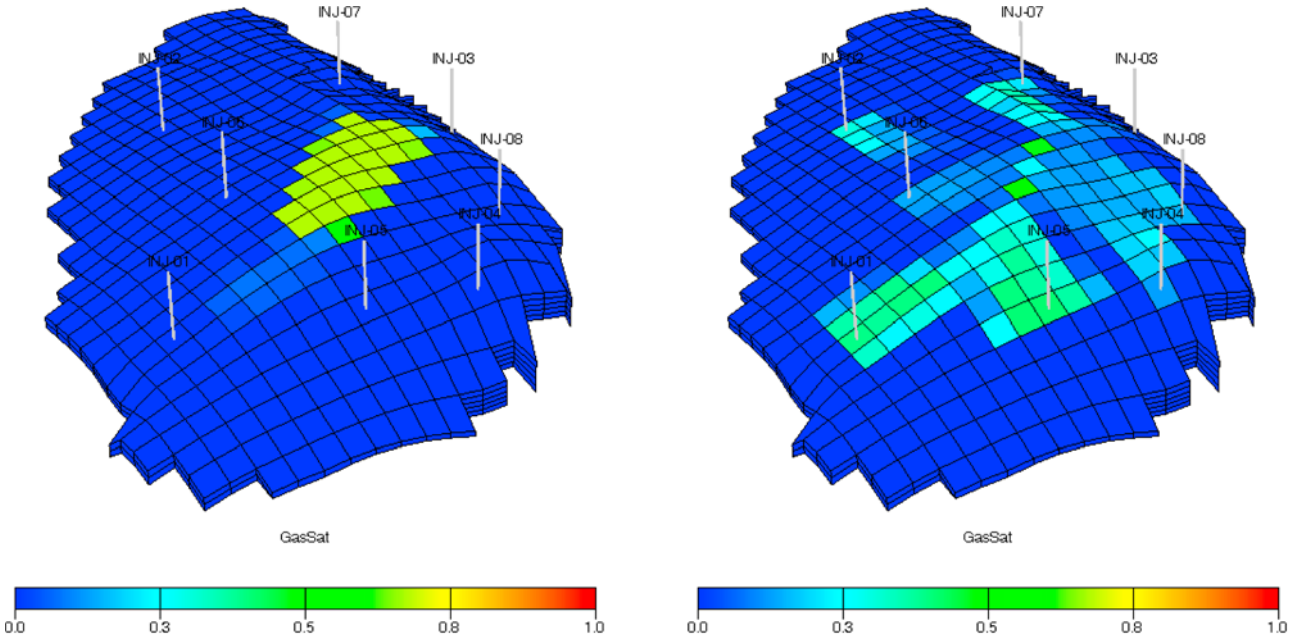

Figure 5. CO_2 saturation distributions after 500 years from the beginning of CO_2 injection. (left) Results from case 1 (no hysteresis). (right) Results from case 2 (with hysteresis).

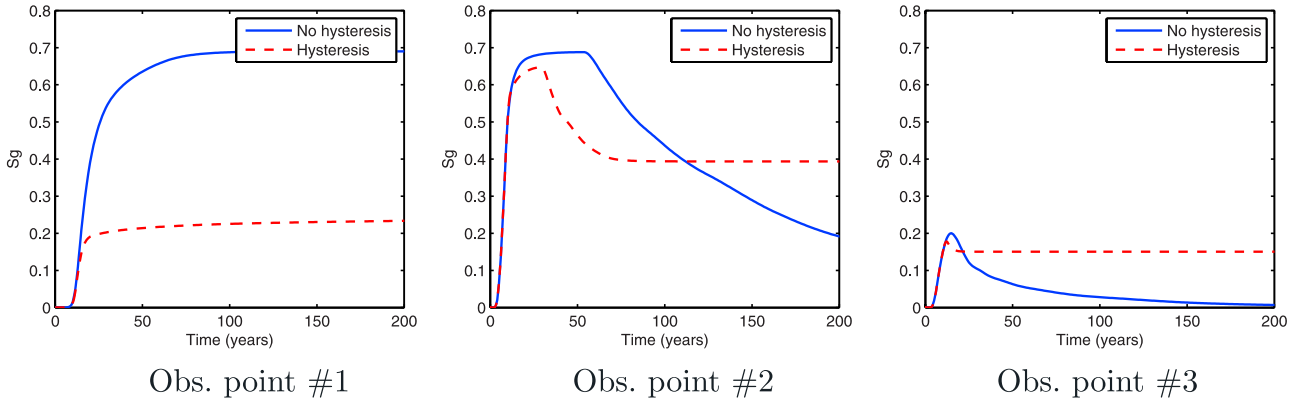

Figure 6. Evolution of actual CO_2 saturations at the three "observation" grid blocks for case 1 (no hysteresis) and case 2 (with hysteresis).

the connate water saturation. In contrast, very little accumulation (CO_2 saturation of about 0.2) occurs when hysteresis is accounted for. The evolution of the CO_2 saturation in blocks at lower elevations (observation points 2 and 3) displays an interesting behavior. When hysteresis is ignored, the gas saturation first increases sharply as the leading edge of the plume reaches the block during its migration upward, and then decreases, eventually to a very low value; the plume travels through the block without leaving any residual CO_2. On the other hand, simulations that account for hysteresis predict that the CO_2 saturation decreases only to a finite, positive value. This is due to trapping during the imbibition process that occurs at the trailing edge of the plume, which results in residual CO_2 being left behind.

[30] These observations are confirmed by the evolution of the trapped CO_2 saturation at the three observation grid blocks, shown in Figure 7. In the model without hysteresis, the trapped CO_2 saturation is of course zero at all times. In the model with hysteresis, the trapped saturation at the top of the anticline (observation point 1) is also equal to zero, because this block only experiences drainage; the actual CO_2 saturation increases with time. At observation points 2 and 3, however, the model predicts that the fraction of trapped CO_2 increases with time. The curve of trapped saturation levels off after 25 years at observation point 3, which is at a lower elevation, and after almost 100 years at observation point 2 (higher elevation) reflecting the different times at which the trailing edge of the plume travels through the different blocks. In these two grid blocks, all the CO_2 present after 100 years is immobile. The value of the ultimate residual CO_2 saturation is related to the maximum CO_2 saturation through the Land trapping relation, equation (1).

4.2. Effect of Injection Rate

[31] We now investigate the effects of CO_2 injection rate on the overall performance of the sequestration project. We do so by comparing cases 2 and 3, both of which account for hysteresis. We inject the same amount of CO_2 in both cases, but over a period of 10 years in case 2 and over a period of 50 years in case 3.

[32] The saturation distributions for both of these cases are shown in Figure 8. Clearly, a slower injection rate (case 3) leads to more mobile CO_2 reaching the top of the aquifer, which has an adverse effect for sequestration purposes. These results can be explained as follows.

[33] Higher injection rates lead to a more radial displacement pattern and higher gas pressures in the vicinity of wells. Physically, this higher pressure is responsible for the nonwetting gas to invade smaller pores, which have a higher

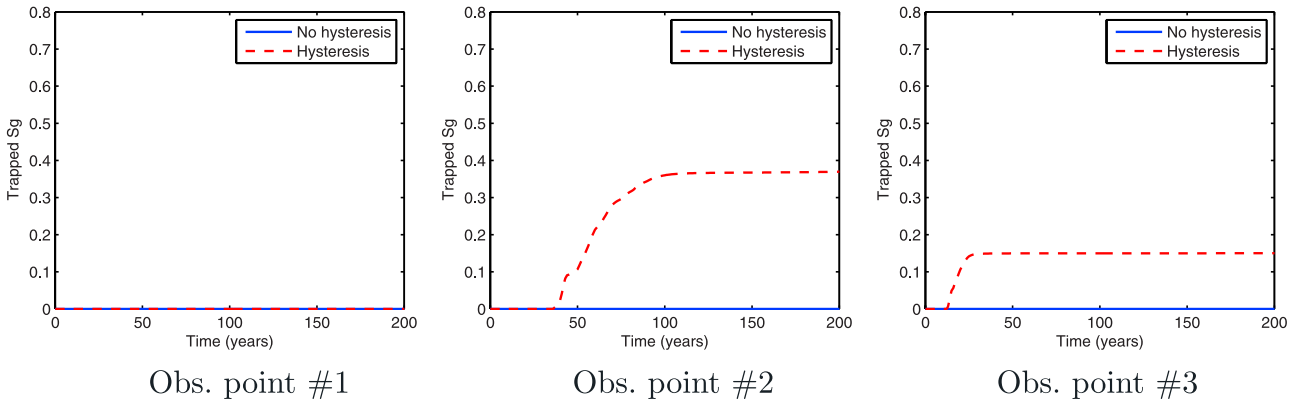

Figure 7. Evolution of trapped CO_2 saturations at the three "observation" grid blocks for case 1 (no hysteresis) and case 2 (with hysteresis).

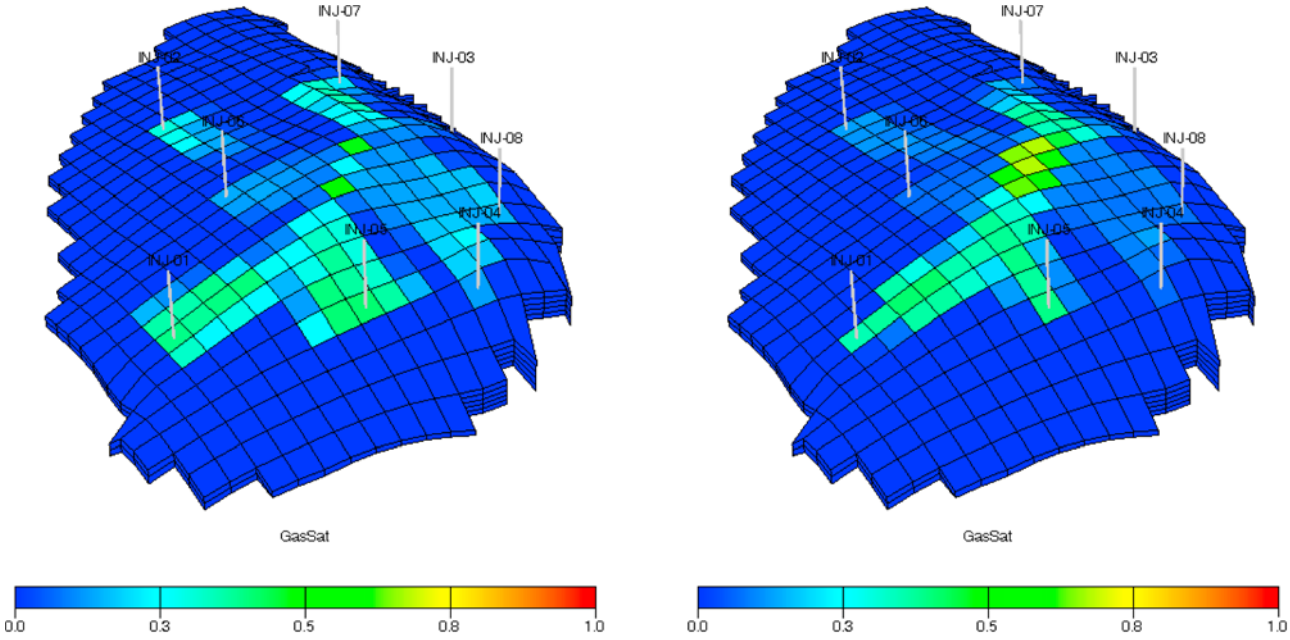

Figure 8. CO_2 saturation distributions after 500 years from the beginning of CO_2 injection. (left) Results from case 2 (injection over 10 years). (right) Results from case 3 (injection over 50 years).

capillary entry pressure. Snap-off occurs readily in smaller pores during imbibition, resulting in increased macroscopic trapping.

[34] For lower injection rates, on the other hand, gravity affects the displacement pattern of water by CO_2 earlier. The low-viscosity gas forms stable paths through the high permeability regions of the porous medium. Microscopically, only the largest pores are invaded, which leads to reduced snap-off during an eventual imbibition process. Moreover, the CO_2 reaches the top of the formation before injection ceases. Since trapping only occurs during imbibition (water displacing CO_2 at the trailing edge of the plume), the fraction of CO_2 that has reached the top of the aquifer cannot undergo imbibition and is therefore not subject to trapping.

[35] The plots of actual and trapped CO_2 saturation over time for these two cases are shown in Figures 9 and 10, respectively. As seen from the plots of observation points 2 and 3, the system undergoes trapping of the CO_2 in both cases. However, the case with low injection rate shows that a higher fraction of CO_2 reaches the top of the anticline (observation point 1): a CO_2 saturation of about 0.7 as opposed to 0.2 of the high-rate injection case.

4.3. Effect of Alternating Water Injection

[36] Finally, we investigate how the performance of the CO_2 sequestration project is affected by the injection of alternating slugs of water and CO_2 into the aquifer. The motivation is to enhance the imbibition process that naturally occurs at the trail of the nonwetting CO_2 plume as it migrates upward.

[37] In Figure 11 we compare the fluid distributions of case 2 and case 4. In both cases we inject 0.15 pore volumes of CO_2 over a period of 10 years. In case 2, the injection of CO_2 is continuous. In case 4, on the other hand, the injection scheme is as follows: 0.075 PV of CO_2 during

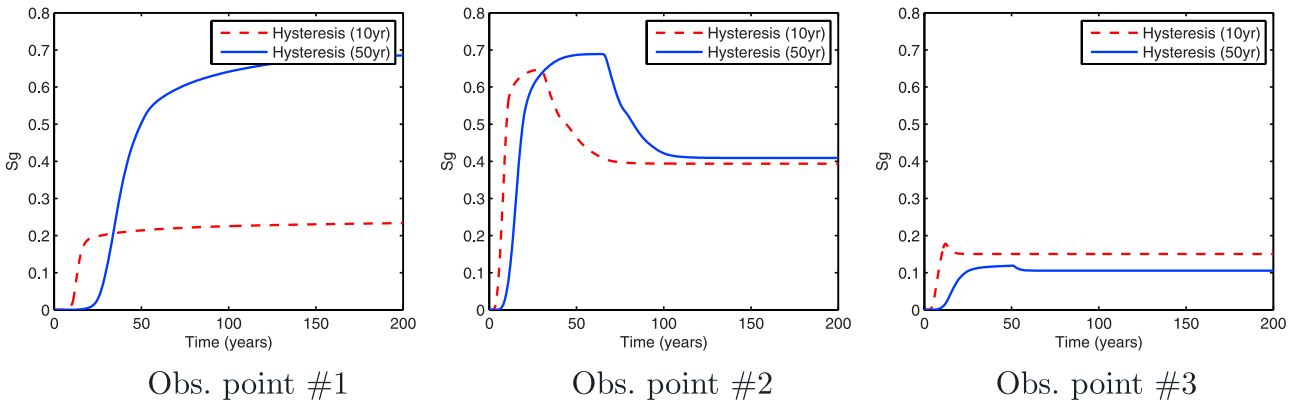

Figure 9. Evolution of actual CO_2 saturations at the three "observation" grid blocks for case 2 (injection over 10 years) and case 3 (injection over 50 years).

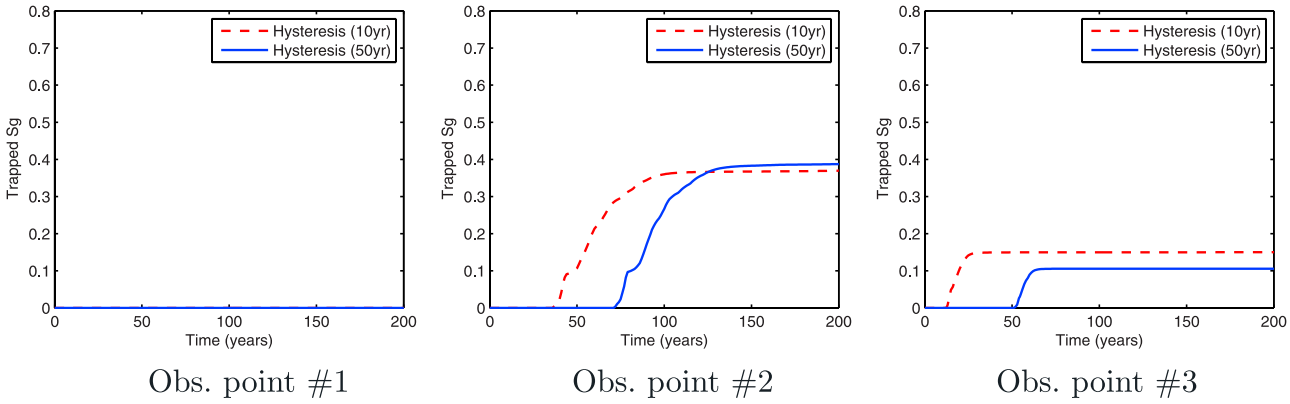

Figure 10. Evolution of trapped CO_2 saturations at the three "observation" grid blocks for case 2 (injection over 10 years) and case 3 (injection over 50 years).

5 years, 0.05 PV of water during one year, 0.075 PV of CO_2 during the next 5 years and, finally, another slug of 0.05 PV of water during one year. The results confirm the expected response: alternating water injection induces more trapping and reduces significantly the amount of CO_2 that accumulates at the top of the aquifer.

[38] The evolution of the actual and trapped CO_2 saturation at the observation grid blocks (Figures 12 and 13, respectively) offers additional insight into the behavior of the displacement process. During the CO_2 injection period, the first 5 years, the curves corresponding to case 2 and case 4 are of course identical. After 5 years, the curves start to deviate due to the injection of water. Water displaces CO_2 radially away from the wells, which can be seen as a forced imbibition process that leads to enhanced trapping. It explains why less CO_2 reaches the top of the aquifer (observation point 1): gas saturation of about 0.1 instead of 0.2 of the continuous CO_2 injection case.

4.4. Impact on the Bottom Hole Pressure

[39] In the previous sections, we illustrated the benefit of higher injection rates and water-alternating-gas injection in terms of increasing residual trapping of CO_2. However, both strategies lead to an increase in the bottom hole pressure (BHP) at the wells, if injection rate is to be maintained.

[40] In this section, we compare the BHP at two of the wells for case 2 (continuous CO_2 injection) and case 4 (water-alternating-gas injection). The evolution of the BHP at two wells during the injection period is shown in Figure 14. The two wells shown, wells 2 and 4, were selected because

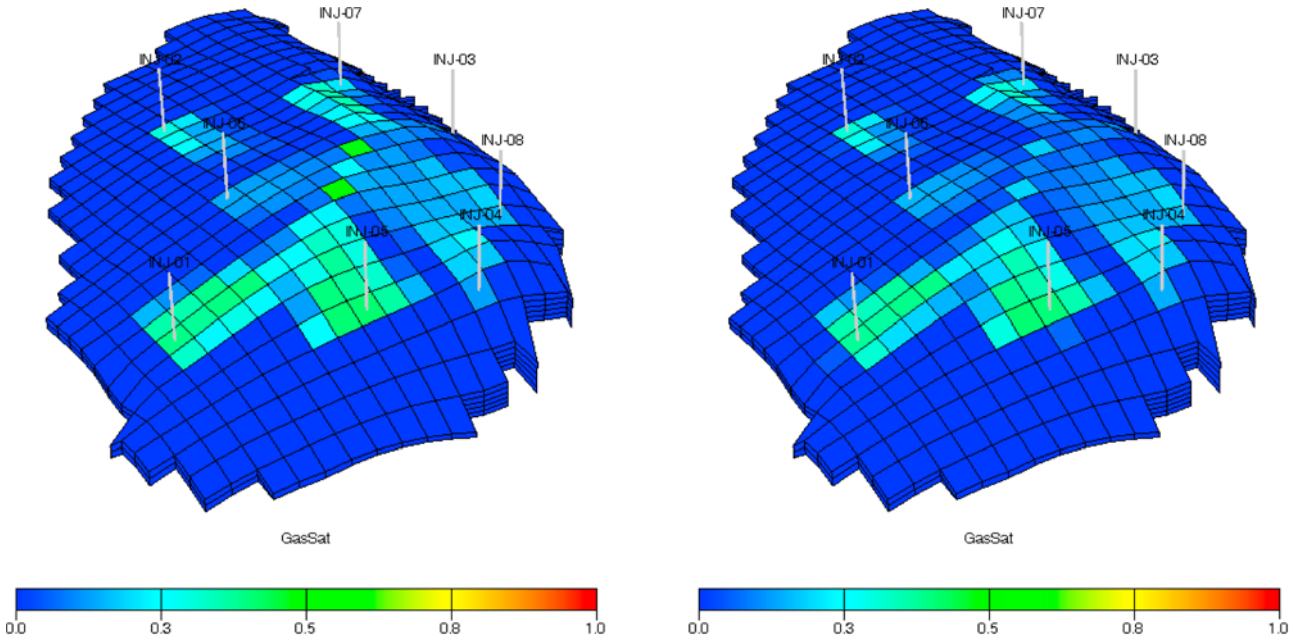

Figure 11. CO_2 saturation distributions after 500 years from the beginning of CO_2 injection. (left) Results from case 2 (no water injection). (right) Results from case 4 (alternating water and CO_2 injection).

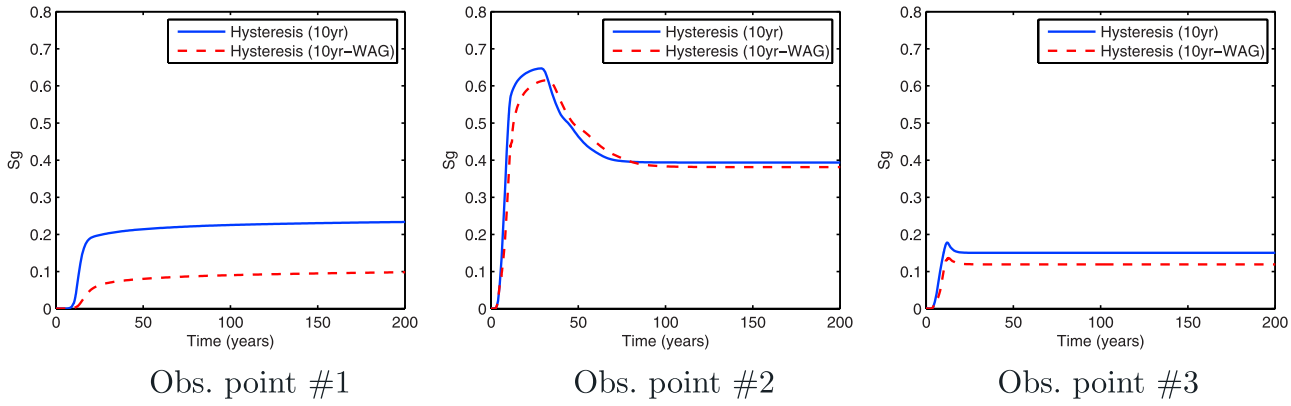

Figure 12. Evolution of actual CO_2 saturations at the three "observation" grid blocks for case 2 (no water injection) and case 4 (alternating water and CO_2 injection).

they display the smallest and largest differences in BHP between the two injection schemes, respectively. It is apparent that a water-alternating-gas strategy results in a significant increase in the operating BHP. The reason is twofold: first, the compressibility of water is much smaller than that of CO_2; moreover, the water injection rate is about three times higher than the injection rate of CO_2. The combined effect is a sudden jump in BHP when water injection starts, and a steeper rate of increase of BHP during water injection. As soon as water injection ceases, the well BHP drops quickly.

[41] The importance of such difference in bottom hole pressure is that BHP is often subject to regulatory limits [*Bachu et al.*, 2003], and a higher BHP also leads to higher operating costs. These factors must be taken into account when establishing the operational benefit of a water-alternating-gas injection strategy.

4.5. Impact of Grid Refinement

[42] The simulations presented so far employ a very coarse discretization (each grid block is approximately $180 \times 180 \times 3$ m^3). Clearly, this crude spatial discretization affects the accuracy of the predictions. In particular, the averaging (or mixing) that takes place at each grid block overestimates the exposure of CO_2 to the pore space during the injection period, thereby overestimating the amount that is trapped during the subsequent imbibition process [*Mo et al.*, 2005].

[43] To illustrate this point, we repeated the simulations using a refined grid in which each grid block is divided into $3 \times 3 \times 3$ grid blocks. This refinement results in a model of about 50,000 active grid blocks. The CO_2 saturation maps after 500 years for case 1 (no hysteresis) and case 2 (with hysteresis) are shown in Figure 15. We show the three-dimensional model up to a vertical cross section, to visualize the vertical CO_2 distribution. When compared with the coarse model in Figure 5 we observe that, for case 2, a higher fraction of CO_2 has reached the top of the anticline. The reason is that a finer discretization captures the overall sweep more accurately, which is overestimated in coarse models. This is particularly relevant here, since the buoyant CO_2 migrates in a relatively thin layer below the reservoir top.

[44] This behavior is also reflected in the evolution of the CO_2 saturation at the observations points (Figure 16). In the refined model, observation point 3 is never contacted by CO_2. At observation point 1, both models (with and without hysteresis) predict the same saturation history, because the CO_2 makes its way to the top of the anticline during (or

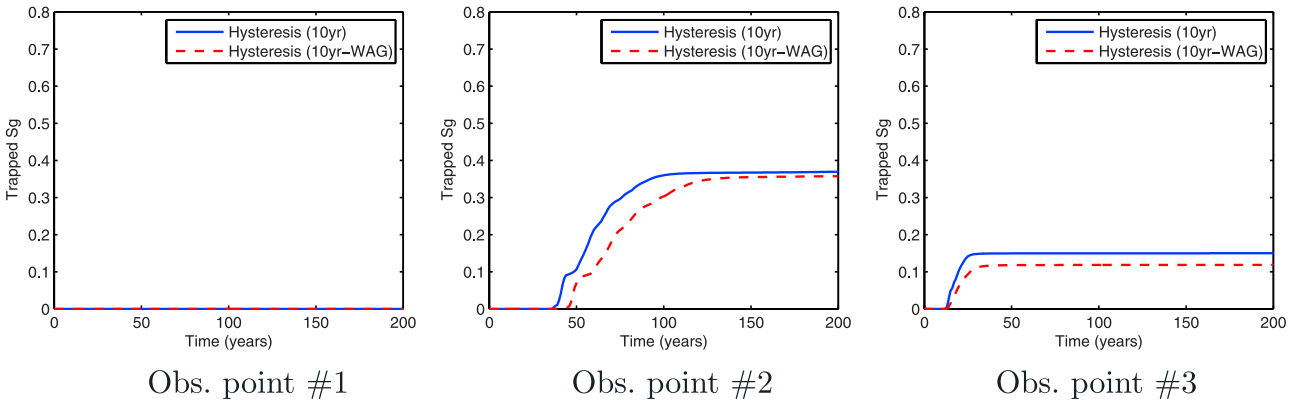

Figure 13. Evolution of trapped CO_2 saturations at the three "observation" grid blocks for case 2 (no water injection) and case 4 (alternating water and CO_2 injection).

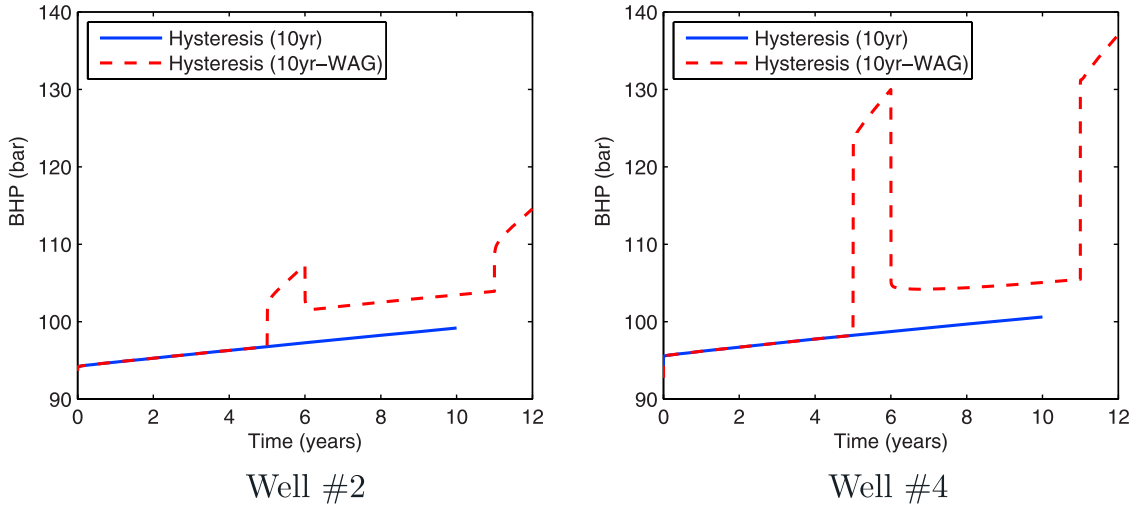

Figure 14. Evolution of bottom hole pressure (BHP) at two different wells for case 2 (continuous CO_2 injection) and case 4 (water-alternating-gas injection).

shortly after) the injection period, from which it cannot be trapped. For observation point 2, however, the simulation shows that wherever the CO_2 plume contacts the reservoir, it will leave a trail of residual immobile gas during its lateral and upward migration.

5. Summary and Conclusions

[45] In this paper, we have investigated the impact of trapping and relative permeability hysteresis in the context of CO_2 sequestration projects in saline aquifers. The main findings can be summarized as follows.

[46] 1. Accounting for trapping and relative permeability hysteresis of the nonwetting CO_2 phase is essential in order to correctly characterize the migration and final distribution of the injected CO_2. Trapping of the CO_2 occurs during the upward migration of the CO_2 plume, but only after injection has stopped and the trailing edge of the plume is naturally being displaced by water. This imbibition process leads to trapping of the CO_2. A trail of residual CO_2 is left behind as the plume migrates upward.

[47] 2. Trapping of the CO_2 leads to more favorable scenarios for sequestration purposes: a large fraction of the CO_2 is trapped and immobile for practical purposes, and is more spread out throughout the aquifer, thereby increasing the interfacial area for subsequent dissolution in the brine. The simulations presented here are representative of a pilot CO_2 injection test, rather than a full-field storage project. Larger volumes per injection well would result in a CO_2 plume that is less distributed across the reservoir, which would result in less capillary trapping. In contrast, target storage formations would likely be thicker,

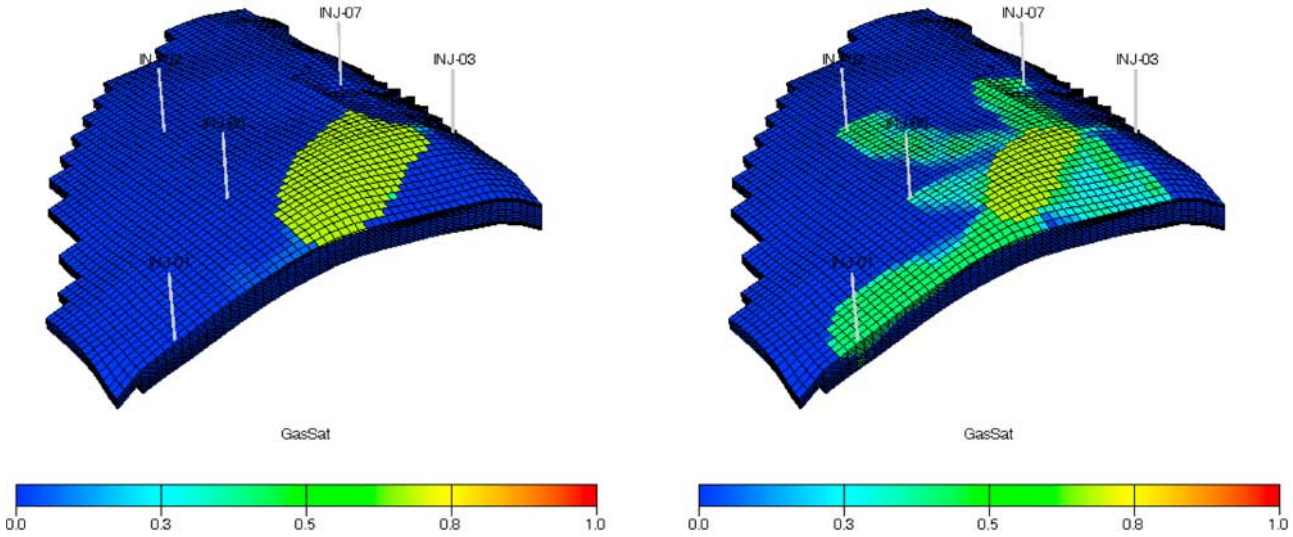

Figure 15. CO_2 saturation distributions after 500 years from the beginning of CO_2 injection, computed on the refined grid. (left) Results from case 1 (no hysteresis). (right) Results from case 2 (with hysteresis).

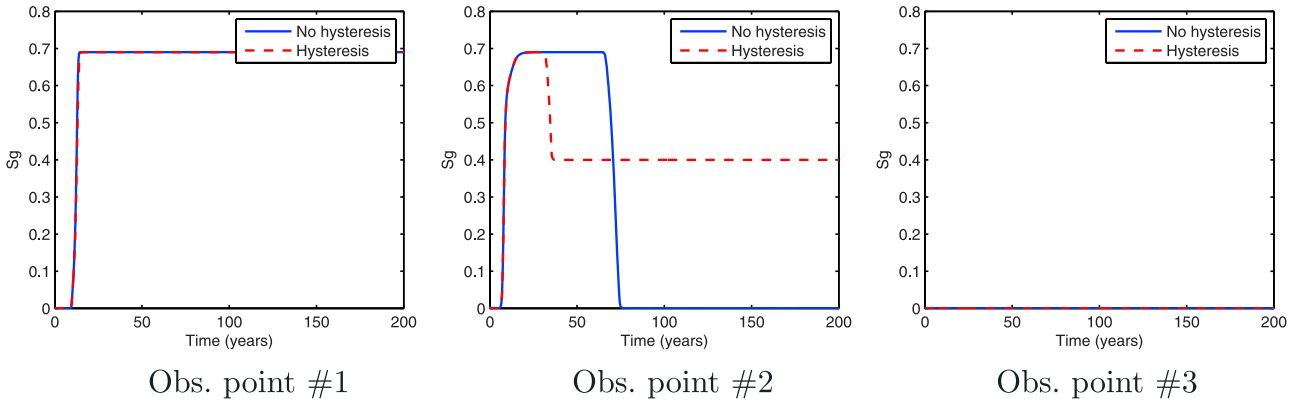

Figure 16. Evolution of actual CO_2 saturations at the three "observation" grid blocks for case 1 (no hysteresis) and case 2 (with hysteresis) from the fine-grid simulation.

sloping aquifers, where the injected CO_2 would continue to rise leaving a trail of residual CO_2 over a larger areal extension.

[48] 3. High injection rates result in more effective sequestration of the CO_2. A shorter injection period leaves less time for the buoyant CO_2 to reach the top of the formation, from which it is difficult to immobilize.

[49] 4. Injection of water slugs alternating CO_2 injection (in the spirit of classical WAG for enhanced oil recovery [*Spiteri and Juanes*, 2006]) increases the effectiveness of the sequestration project. The injected water forces breakup of large connected CO_2 plumes, enhancing trapping and immobilization of the CO_2. On the other hand, a WAG strategy leads to higher bottom hole pressures at injection wells, which may be limited by seal integrity, regulatory or economical constraints. The identification of WAG as a potentially effective strategy for CO_2 storage lends itself to an optimization problem to maximize the amount of trapped CO_2 by varying the well rates and well completions, subject to BHP constraints.

[50] 5. Coarse simulation models overestimate the sweep and subsequent capillary trapping of CO_2. We believe that an accurate assessment of the different storage mechanisms (hydrodynamic, capillary, solution and mineral trapping) requires high-resolution models that capture the migration paths of the injected CO_2 in the subsurface.

[51] **Acknowledgments.** The authors gratefully acknowledge financial support from the industrial affiliates of the Stanford University Petroleum Research Institute for Gas Injection (SUPRI-C) and support from the Global Climate and Energy Project (GCEP). We thank the reviewers for their insightful comments, which led to a substantial improvement of the paper.

References

Al-Futaisi, A., and T. W. Patzek (2003), Impact of wettability on two-phase flow characteristics of sedimentary rock: A quasi-static description, *Water Resour. Res.*, *39*(2), 1042, doi:10.1029/2002WR001366.

Aziz, K., and A. Settari (1979), *Petroleum Reservoir Simulation*, Elsevier, New York.

Bachu, S. (2000), Sequestration of CO_2 in geological media: Criteria and approach for site selection in response to climate change, *Energy Convers. Manage.*, *41*(9), 953–970.

Bachu, S. (2003), Sequestration of CO_2 in geological media in response to climate change: Capacity of deep saline aquifers to sequester CO_2 in solution, *Energy Convers. Manage.*, *44*(20), 3151–3175.

Bachu, S., W. D. Gunther, and E. H. Perkins (1994), Aquifer disposal of CO_2: Hydrodynamic and mineral trapping, *Energy Convers. Manage.*, *35*(4), 269–279.

Bachu, S., K. Haug, K. Michael, B. E. Buschkuehle, and J. J. Adams (2003), Deep injection of acid gas in Western Canada, paper presented at Second International Symposium on Underground Injection Science and Technology, Lawrence Berkeley Natl. Lab., Berkeley, Calif.

Bennion, D. B., and S. Bachu (2006), Supercritical CO_2 and H_2S—Brine drainage and imbibition relative permeability relationships for intergranular sandstone and carbonate formations, *SPE Pap. 99326*, Soc. of Pet. Eng., Richardson, Tex.

Blunt, M. J. (2000), An empirical model for three-phase relative permeability, *Soc. Pet. Eng. J.*, *5*(4), 435–445.

Bromhal, G. S., W. N. Sams, S. Jikich, T. Ertekin, and D. H. Smith (2005), Simulation of CO_2 sequestration in coal beds: The effects of sorption isotherms, *Chem. Geol.*, *217*(3–4), 201–211.

Bruant, R. G., Jr., M. A. Celia, A. J. Guswa, and C. A. Peters (2002), Safe storage of CO_2 in deep saline aquifers, *Environ. Sci. Technol.*, *36*(11), 240A–245A.

Carlson, F. M. (1981), Simulation of relative permeability hysteresis to the nonwetting phase, *SPE Pap. 10157-MS*, Soc. of Pet. Eng., Richardson, Tex.

Cox, P. M., R. A. Betts, C. D. Jones, S. A. Spall, and I. J. Totterdell (2000), Acceleration of global warming due to carbon-cycle feedbacks in a coupled climate model, *Nature*, *408*(6809), 184–187.

de Gennes, P.-G., F. Brochard-Wyart, and D. Quere (2004), *Capillarity and Wetting Phenomena: Drops, Bubbles, Pearls, Waves*, Springer, New York.

Doughty, C., and K. Pruess (2004), Modeling supercritical carbon dioxide injection in heterogeneous porous media, *Vadose Zone J.*, *3*, 837–847.

Ennis-King, J., and L. Paterson (2002), Engineering aspects of geological sequestration of carbon dioxide, *SPE Pap. 77809-MS*, Soc. of Pet. Eng., Richardson, Tex.

Ennis-King, J., and L. Paterson (2005), Role of convective mixing in the long-term storage of carbon dioxide in deep saline formations, *Soc. Pet. Eng. J.*, *10*(3), 349–356.

Ennis-King, J., I. Preston, and L. Paterson (2005), Onset of convection in anisotropic porous media subject to a rapid change in boundary conditions, *Phys. Fluids*, *17*(8), 084107, doi:10.1063/1.2033911.

Falkowski, P., et al. (2000), The global carbon cycle: A test of our knowledge of Earth as a system, *Science*, *290*(5490), 291–296.

Flett, M., R. Gurton, and I. Taggart (2004), The function of gas–water relative permeability hysteresis in the sequestration of carbon dioxide in saline formations, *SPE Pap. 88485-MS*, Soc. of Pet. Eng., Richardson, Tex.

Floris, F. J. T., M. D. Bush, M. Cuypers, F. Roggero, and A. R. Syversveen (2001), Methods for quantifying the uncertainty of production forecasts: A comparative study, *Petrol. Geosci.*, *7*, S87–S96.

Garcia, J. E. (2003), Fluid dynamics of carbon dioxide disposal into saline aquifers, Ph.D. dissertation, Univ. of Calif., Berkeley.

Gunter, W. D., B. Wiwchar, and E. H. Perkins (1997), Aquifer disposal of CO_2-rich greenhouse gases: Extension of the time scale of experiment for CO_2-sequestering reactions by geochemical modeling, *Miner. Petrol.*, *59*(1–2), 121–140.

Hitchon, G., W. D. Gunter, T. Gentzis, and R. T. Bailey (1999), Sedimentary basins and greenhouse gases: A serendipitous association, *Energy Convers. Manage.*, *40*(8), 825–843.

Hoffert, M. I., et al. (1998), Energy implications of future stabilization of atmospheric CO_2 content, *Nature*, *395*(6704), 881–884.

Holloway, S. (2001), Storage of fossil fuel-derived carbon dioxide beneath the surface of the earth, *Annu. Rev. Energy Environ.*, *26*, 145–166.

Hovorka, S. D., C. Doughty, and M. H. Holtz (2004), Testing efficiency of storage in the subsurface: Frio brine pilot experiment, paper presented at International Conference on Greenhouse Gas Control Technologies (GHGT-7), Int. Energy Agency, Vancouver, B. C., Canada.

Hunt, J. R., N. Sitar, and K. S. Udell (1988), Nonaqueous phase liquid transport and cleanup: 1. Analysis of mechanisms, *Water Resour. Res.*, *24*(8), 1247–1258.

Intergovernmental Panel on Climate Change, (1996). *Climate Change 1995: The Science of Climate Change*, edited by J. T. Houghton et al., Cambridge Univ. Press, New York.

Jerauld, G. R. (1997), General three-phase relative permeability model for Prudhoe Bay, *SPE Reservoir Eval. Eng.*, *12*(4), 255–263.

Jerauld, G. R., and S. J. Salter (1990), Effect of pore-structure on hysteresis in relative permeability and capillary pressure: Pore-level modeling, *Transp. Porous Media*, *5*, 103–151.

Jimenez, J. A., and R. J. Chalaturnyk (2002), Integrity of bounding seals for geologic storage of greenhouse gases, *SPE Pap. 78196*, Soc. of Pet. Eng., Richardson, Tex.

Johnson, J. W., C. I. Steefel, J. J. Nitao, and K. G. Knauss (2000), Reactive transport modeling of subsurface CO_2 sequestration: Identification of optimal target reservoirs and evaluation of performance based on geochemical, hydrologic and structural constraints, paper presented at Energex 2000, 8th International Forum, Int. Energy Found., Las Vegas, Nevada.

Killough, J. E. (1976), Reservoir simulation with history-dependent saturation functions, *Soc. Pet. Eng. J.*, *16*(1), 37–48.

Knauss, K. G., J. W. Johnson, and C. I. Steefel (2005), Evaluation of the impact of CO_2, co-contaminant gas, aqueous fluid and reservoir rock interactions on the geologic sequestration of CO_2, *Chem. Geol.*, *217*(3–4), 339–350.

Kovscek, A. R., and M. D. Cakici (2005), Geologic storage of carbon dioxide and enhanced oil recovery. II. Cooptimization of storage and recovery, *Energy Convers. Manage.*, *46*, 1941–1956.

Kovscek, A. R., and Y. Wang (2005), Geologic storage of carbon dioxide and enhanced oil recovery. I. Uncertainty quantification employing a streamline based proxy for reservoir flow simulation, *Energy Convers. Manage.*, *46*, 1920–1940.

Kumar, A., R. Ozah, M. Noh, G. A. Pope, S. Bryant, K. Sepehrnoori, and L. W. Lake (2005), Reservoir simulation of CO_2 storage in deep saline aquifers, *Soc. Pet. Eng. J.*, *10*(3), 336–348.

Lackner, K. S. (2003), A guide to CO_2 sequestration, *Science*, *300*(5626), 1677–1678.

Land, C. S. (1968), Calculation of imbibition relative permeability for two- and three-phase flow from rock properties, *Soc. Pet. Eng. J.*, *8*(2), 149–156.

Larsen, J. A., and A. Skauge (1998), Methodology for numerical simulation with cycle-dependent relative permeabilities, *Soc. Pet. Eng. J.*, *3*(2), 163–173.

Lenhard, R. J., and M. Oostrom (1998), A parametric model for predicting relative permeability-saturation-capillary pressure relationships of oil-water systems in porous media with mixed wettability, *Transp. Porous Media*, *31*, 109–131.

Lenhard, R. J., and J. C. Parker (1987), A model for hysteretic constitutive relations governing multiphase flow: 2. Permeability-saturation relations, *Water Resour. Res.*, *23*(12), 2197–2206.

Lenormand, R., C. Zarcone, and A. Sarr (1983), Mechanisms of the displacement of one fluid by another in a network of capillary ducts, *J. Fluid Mech.*, *135*, 123–132.

McCain, W. D., Jr. (1990), *The Properties of Petroleum Fluids*, PennWell Books, Tulsa, Okla.

Mo, S., and I. Akervoll (2005), Modeling long-term CO_2 storage in aquifer with a black-oil reservoir simulator, *SPE Pap. 93951-MS*, Soc. of Pet. Eng., Richardson, Tex.

Mo, S., P. Zweigel, E. Lindeberg, and I. Akervoll (2005), Effect of geologic parameters on CO_2 storage in deep saline aquifers, in *14th Europec Biennial Conference*, Madrid, Spain, (SPE 93952).

Nordbotten, J. M., M. A. Celia, and S. Bachu (2004), Analytical solutions for leakage rates through abandoned wells, *Water Resour. Res.*, *40*, W04204, doi:10.1029/2003WR002997.

Oak, M. J. (1990), Three-phase relative permeability of water-wet Berea, *SPE Pap. 20183-MS*, Soc. of Pet. Eng., Richardson, Tex, (SPE/DOE 20183).

Obi, E.-O. I., and M. J. Blunt (2006), Streamline-based simulation of carbon dioxide storage in a North Sea aquifer, *Water Resour. Res.*, *42*, W03414, doi:10.1029/2004WR003347.

Orr, F. M., Jr. (2004), Storage of carbon dioxide in geologic formations, *J. Pet. Technol.*, *56*(9), 90–97.

Pruess, K., and J. García (2002), Multiphase flow dynamics during CO_2 disposal into saline aquifers, *Environ. Geol.*, *42*(2–3), 282–295.

Pruess, K., T. Xu, J. Apps, and J. Garcia (2003), Numerical modeling of aquifer disposal of CO_2, *Soc. Pet. Eng. J.*, *8*(1), 49–60.

Riaz, A., M. Hesse, H. A. Tchelepi, and F. M. Orr Jr. (2006), Onset of convection in a gravitationally unstable, diffusive boundary layer in porous media, *J. Fluid Mech.*, *548*, 87–111.

Rutqvist, J., and C. F. Tsang (2002), A study of caprock hydromechanical changes associated with CO_2 injection into a brine formation, *Environ. Geol.*, *42*(2–3), 296–305.

Schlumberger (2005), Eclipse technical description, v. 2005A, report, Abingdon, U. K.

Spiteri, E. J., and R. Juanes (2006), Impact of relative permeability hysteresis on the numerical simulation of WAG injection, *J. Pet. Sci. Eng.*, *50*(2), 115–139.

Spiteri, E. J., R. Juanes, M. J. Blunt, and F. M. Orr Jr. (2005), Relative permeability hysteresis: Trapping models and application to geological CO_2 sequestration, in *SPE Annual Technical Conference and Exhibition*, Dallas, TX, (SPE 96448).

Valvatne, P. H., and M. J. Blunt (2004), Predictive pore-scale modeling of two-phase flow in mixed wet media, *Water Resour. Res.*, *40*, W07406, doi:10.1029/2003WR002627.

Wellman, T. P., R. B. Grigg, B. J. McPherson, R. K. Svec, and P. C. Lichtner (2003), The evaluation of CO_2–brine-rock interaction with laboratory flow test and reactive transport modeling, in *SPE/DOE International Symposium on Oilfield Chemistry*, Houston, Texas, (SPE 80228).

Wigley, T. M. L., R. Richels, and J. A. Edmonds (1996), Economic and environmental choices in the stabilization of atmospheric CO_2 concentrations, *Nature*, *379*(6562), 240–243.

Xu, T. F., J. A. Apps, and K. Pruess (2003), Reactive geochemical transport simulation to study mineral trapping for CO_2 disposal in deep arenaceous formations, *J. Geophys. Res.*, *108*(B2), 2071, doi:10.1029/2002JB001979.

M. J. Blunt, Department of Earth Science and Engineering, Imperial College London, London SW7 2AZ, UK. (m.blunt@imperial.ac.uk)

R. Juanes, Department of Civil and Environmental Engineering, Massachusetts Institute of Technology, 77 Massachusetts Avenue, Building 48, Cambridge, MA 02139, USA. (juanes@mit.edu)

F. M. Orr Jr., Department of Petroleum Engineering, Stanford University, 65 Green Earth Sciences Building, Stanford, CA 94305, USA. (fmorr@stanford.edu)

E. J. Spiteri, Chevron Energy Technology Company, 1500 Louisiana Street, Houston, TX 77002, USA. (espiteri@chevron.com)